BIOCYBERNETICS AND BIOMEDICALENGINEERING 41 (2021) 704–716

Available at www.sciencedirect.com

ScienceDirect

journal homepage: www.elsevier.com/locate/bbe

Original Research Article

Detection of subthalamic nucleus using novel higher-order spectra features in microelectrode recordings signals

Mohamed Hosny [a,c,1], *Minwei Zhu* [b,1], *Wenpeng Gao* [a,*], *Yili Fu* [a]

[a] *School of Life Science and Technology, Harbin Institute of Technology, 2 Yikuang Str., Nangang District, Harbin 150080, China*

[b] *Department of Neurosurgery, First Affiliated Hospital of Harbin Medical University, 23 Youzheng Str., Nangang District, Harbin 150001, China*

[c] *Department of Electrical Engineering, Benha faculty of engineering, Benha University, Benha, Egypt*

ARTICLE INFO

Article history:
Received 27 March 2020
Received in revised form
4 April 2021
Accepted 29 April 2021
Available online 16 May 2021

Keywords:
Higher-order statistics and spectra
Microelectrode recording
Parkinson's disease
Subthalamic nucleus detection
Deep brain stimulation
Machine learning

ABSTRACT

Successful deep brain stimulation surgery for Parkinson's disease (PD) patients hinges on accurate clustering of the functional regions along the electrode insertion trajectory. Microelectrode recording (MER) is employed as a substantial tool for neuro-navigation and localizing the optimal target, such as the subthalamic nucleus (STN), intraoperatively. MER signals deliver a framework to reveal the underlying characteristics of STN. The motivation behind this work is to explore the application of Higher-order statistics and spectra (HOS) for an automated delineation of the neurophysiological borders of STN using MER signals. Database collected from 21 PD patients were used. Two HOS methods (Bispectrum and cumulant) were exploited to probe non-Gaussian properties of STN region. This is followed by utilizing classifiers, namely K-nearest neighbor, decision tree, Boosting and support vector machine (SVM), to choose the superior classifier. Comparison of the performance achieved via HOS alongside the state-of-the-art techniques shows that the proposed features are better suited for identifying STN borders and achieve higher results. Average classification accuracy, sensitivity, specificity, area under the curve and Youden's J statistics of 94.81%, 96.73%, 92.15%, 0.9444% and 0.8888, respectively, were yielded using SVM with 8 bispectrum and 241 cumulants features. The proposed model can aid the neurosurgeon in STN detection.

* Corresponding author at: Building 2E, Science park of Harbin Institute of Technology, Yikuang Str. 2, Nangang district, Harbin 150080, China.
E-mail address: wpgao@hit.edu.cn (W. Gao).

[1] These authors contributed equally to this work.

https://doi.org/10.1016/j.bbe.2021.04.016

1. Introduction

Parkinson's disease (PD) is a long-term progressive, neurodegenerative disorder caused by the death of cells in the basal ganglia (BG) region [1]. Death of cells causes deficiency of dopamine which is responsible for controlling the human body movements [2,3]. As a result, communication modes in the brain are affected [4]. PD affects people over the age of sixty years old [5]. PD is characterized by major symptoms that include stiffness, bradykinesia [6], resting muscle tremor [7,8], rigidity [9] and sleep disorders [10]. Therefore, deep brain stimulation (DBS) surgery is increasingly being used for alleviating symptoms of advanced PD patients whose condition has worsened or who are no longer reactive to drug treatment [11–13].

DBS is an interventional treatment which encompasses implantation of an electrode in either subthalamic nucleus (STN) [14] or the internal segment of the globus pallidus (GPi) [15,16], in order to deliver high frequency electrical impulses to these specific targets [17]. Therefore, efficient therapeutic effect of DBS hinges on localizing the target structure within the brain with a high accuracy such as, the stimulation of adjacent functional regions has been demonstrated to cause adverse side effects on motor [18], emotional and cognitive functions [10]. Besides, inaccurate positioning of DBS electrodes causes up to 40% of cases with insufficient postoperative stimulation effectiveness [19,20]. Dorsolateral somatosensory region inside the STN is found to be the best place to apply stimulation for PD patients [21].

The most common modalities used to plan for electrode insertion trajectory include, magnetic resonance imaging (MRI) and computer tomography (CT) scans [22]. However, due to resolution limitations of neuroimaging [23], additional adjunctive information from intraoperative guidance is essential. Consequently, MER is employed in real time testing during DBS surgery for validating the planned trajectories in an effort to achieve optimal positioning of electrodes inside the target structure [24]. Additionally, intraoperative delineation of STN borders and its surrounding structures using MER signals can reduce targeting errors by overcoming brain deformation and account for anatomic shifts due to cerebrospinal fluid leakage [25]. MER allows capturing extracellular electric activity of neurons in the closest vicinity of electrodes with a tip size around 1 μm, then, the time domain behavior is inferred intraoperatively by a trained neurologist and/or neurosurgeon while listening to the signal through speakers [26].

Nevertheless, mental interpretation of MER signals for STN segmentation possess several challenges such as, they are non-stationary and have complex signal patterns [27]. Also, there is a difficulty in visual inspection of MER signals due to the presence of artifacts from several sources such as, devices in the operating room, patient speech, electrode movement and blood [26]. Besides, anatomic challenges including that STN has a small size (about 4*7*9 mm), is deep located in the brain and surrounded by structures, for instance, substantia nigra (SNr) and zona incerta (ZI) [28]. Furthermore, uninterrupted transition from STN to SNr and the presence of white matter gaps may lead to wrong labeling of STN exit [29]. Moreover, it is time consuming and there is a critical reliance on subjective evaluation and judgement which could result inconsistencies in MER analysis for STN identification [30]. Therefore, automation of STN borders detection is very important to elude the aforementioned challenges, reduce the surgery time and improve patient comfort during the surgery [31].

In recent years, identification of STN region using MER signals has drawn substantial attention of many researchers, such as, MER analysis using either linear or non-linear techniques could depict inherent biomarkers of STN, which can reveal neural mechanisms in PD patients and show a quantifiable target to implant the DBS electrodes [32]. Feature extraction is considered to be a significant stage in the STN localization model. Meaningful features will maximize the performance of the automation process to outline the dorsal as well as the ventral borders of STN. Researchers have proposed several methods for STN localization using numerous features, ranging from spike dependent (SD) to spike independent (SI) features or combination of them [19]. Wong et al. [33] extracted multiple SD and SI features then, fed them to an unsupervised machine learning approach to identify the STN borders. They suggested that using different combinations of features may ameliorate the system performance. In this regard, Cagnan et al. [30] utilized firing rate, background neural activity in addition to power spectral density (PSD) of low, beta and gamma band indices with corresponding frequencies of (3–12 Hz), (13–30 Hz) and (31–100 Hz), in that order. Higher values in STN region were shown in all the features except for PSD of low band. They obtained an accuracy of 88% in comparison to surgical annotations. Also, Ciecierski et al. extracted a combination of SD attributes (e.g. modified burst ratio and spike frequency) and background neural features (e.g. root mean square (RMS), amplitude and frequency power in 0–500 Hz and 500–3000 Hz) with rough set exploration system (RSES) and random forest (RF) classifier [31] as well as k-means and hierarchical clustering algorithms [34] for STN segmentation. Schiaffino et al. [35] employed 15 SD and SI features with fuzzy k-Nearest Neighbour (KNN) and accomplished sensitivity and specificity of 72% and 82%, respectively. Similarly, in [25], decision trees (DT), Bayesian and KNN classifiers based on 13 SD and SI features were utilized for automated clustering of STN, SNr and ZI. DT with Gini and Max Deviance indices obtained highest accuracy of 87.55% and 89.6%, separately. On the other hand, Bayesian and KNN achieved highest accuracy of 82.84% and 82.25%, correspondingly. Therefore, they reported that feature addition can improve system performance to a certain limit due to the fact that any inappropriate or redundant features would decrease the classification accuracy. This emphasizes that not all the features used in their model were convenient. As a result, they suggested that feature selection is crucial for reliable STN localization framework [19].

Accordingly, Rajpurohit et al. [36] exploited feature selection and patient-specific normalization approaches with logistic regression (LR) classifier to achieve an increase of 38.92 in terms of accuracy compared with using all the features. Authors in [37] investigated up on previous study [35] and used Branch & Bound algorithm to select 6 out of 16

features and inputted them to KNN classifier, obtaining a detection accuracy of 86.13%. In [38], backward and forward wrapper techniques were used for feature selection, resulting decreased classification error of 1.21% and 1.13%, in that order. Also, the number of selected features was one third of the total 18 features, which would decrease the execution time and improve the computational efficiency of their model.

Traditional spectral methods (e.g. PSD and fast Fourier transform (FFT)) were applied in previous studies to probe vital signatures of STN region using MER signals. Valsky et al. [29] revealed a high discrimination between STN and SNr in two frequency ranges (i.e. low frequency range 5–25 Hz and high frequency range 100–150 Hz). Consequently, they developed a new feature which is the ratio of the mean power of the two aforementioned frequency ranges. They were able to identify STN with accuracy of 94% using hidden Markov model (HMM). Khosravi et al. [39] employed FFT for feature extraction from MER signals. They implied that, unlike traditional features [36], FFT has the ability to highlight the alterations in spike activities. Besides, FFT may be more informative and achieved 85% accuracy using LR classifier. They also validated the extracted features using an unsupervised technique, combination of K-means clustering and self-organized map (SOM), to obtain an accuracy of 80% [40]. However, Chaovalitwongse et al. [25] reported against frequency based features, indicating that the frequency components of MER data alone do not provide crucial information of STN region, because the performance of all classifiers were lower than 50%. In addition, the accuracy of the best performing classifier (DT) dropped by 41.86% when compared with employing a combination of SD and SI features.

Meanwhile, focus on MER signals classification using time–frequency analysis is on the rise. Several algorithms which have the advantage of displaying the frequency profile and maintaining excellent frequency resolution, were exploited for the development of accurate STN localization strategies [41,28,27,42]. Authors in [41] found a significant difference between STN and non-STN regions in the two detailed wavelet coefficients sub-bands D1 and D2 with the corresponding MER frequency ranges of 3–6 kHz and 1.5–3 kHz, individually. Such as, the entropy calculated from these coefficients are higher in STN, probably due to the more irregularity of MER signals originate form STN in these frequency ranges. Highest accuracy of 83% was acquired by RF classifier. In their contribution, the work of Vargas Cardona et al. [27] has led to the development of an automated method for STN segmentation problem using inter-spike interval (ISI), adaptive wavelets and wavelet transform (WT). For classification, they used multi-task Gaussian process regression with the linear model of coregionalization (LMC), intrinsic coregionalization model (ICM) and convolved multiple output covariance (CMOC), and achieved the accuracy of 85.99% and 84.1% using two different datasets. In parallel, in 2020, Karthick et al. [28] reported the use of machine learning classifiers based on wavelet packet decomposition (WPD) features to delineate the neurophysiological borders of STN in MER signals. As reported therein, additional information of low and high frequency components can be assembled by WPD approach. Their method yielded average classification accuracy of 94%.

Recently, higher-order statistics and spectra (HOS) technique has been commonly used to extract subtle variations in bio-signals and achieved promising results in various applications for instance, PD diagnosis [43], seizure prediction [44] and identification of coronary artery disease [45]. Despite that, HOS has not yet been applied to MER signals of PD patients for STN segmentation. Consequently, this study concentrates on exploiting HOS to discover the hidden non-linear parameters and understand the neural basis from MER signals which are essential to enable the automated detection of STN region. The work flow of the proposed system is displayed in Fig. 1. After segmentation and preprocessing of MER signals, the features are extracted using HOS and classified by several machine learning classifiers. Furthermore, in this study, we have extracted two groups of features, which were reported in the scientific literature discussed earlier, in order to confront the performance of the proposed HOS features with the existing methods in the field of MER analysis. The first group is the state-of-the-art nine SD and SI features reported in [36,40,46,38,25]. The second group is the WPD based features suggested in [28] as a reliable source of information for classifying the MER signals originate from inside and outside the STN region based on the electrophysiological activity. The aforementioned two groups of features in addition to the developed HOS features were fed to 10 machine learning classifiers. The results of the comparative study show that the proposed HOS model improved the classification efficacy in comparison to the existing methods.

2. MER recordings and surgical procedure

In this study, MER data were recorded for electrophysiological exploration of idiopathic PD patients during DBS surgery. Data were collected from the First Affiliated Hospital of Harbin Medical University, Harbin, China. The collected data comprised of 832 single channel recordings obtained from 21 patients (11 males and 10 females; age: 65.1 ± 5.6 years). Among them, 18 patients were inserted in both hemispheres (bilaterally) and only 3 patients were inserted unilaterally, therefore, data included 39 MER trajectories. Table 1 describes MER data used in this study.

All patients were implanted in STN using one microelectrode (Medtronic, Inc.). MER signals were recorded using the MicroGuide system (AlphaOmega Engineering, Nazareth, Israel) at a sampling rate of 24 kHz, 8-bit converter and a total gain of 10000. MER recordings were labeled according to their corresponding location (i.e. whether inside or outside STN) into two classes (STN and non-STN). Total length of MERs are 5273 s (over 1 h and 27 min), among this, 3206 s are associated with STN region, while the rest 2067 s stem from non-STN region. All patients discontinued taking long-acting and short-acting dopaminergic medications 72 and 12 h prior to the surgery, in that order. Also, they had established at least 30% improvement in the unified Parkinson's disease rating scale (UPDRS), and were awake during the surgery. Data collection was considered to be a part of an unaltered standard surgical procedure.

Surgical planning is based on fusion between preoperative 1.5T MRI (T1 and T2 weighted) and intraoperative stereotactic

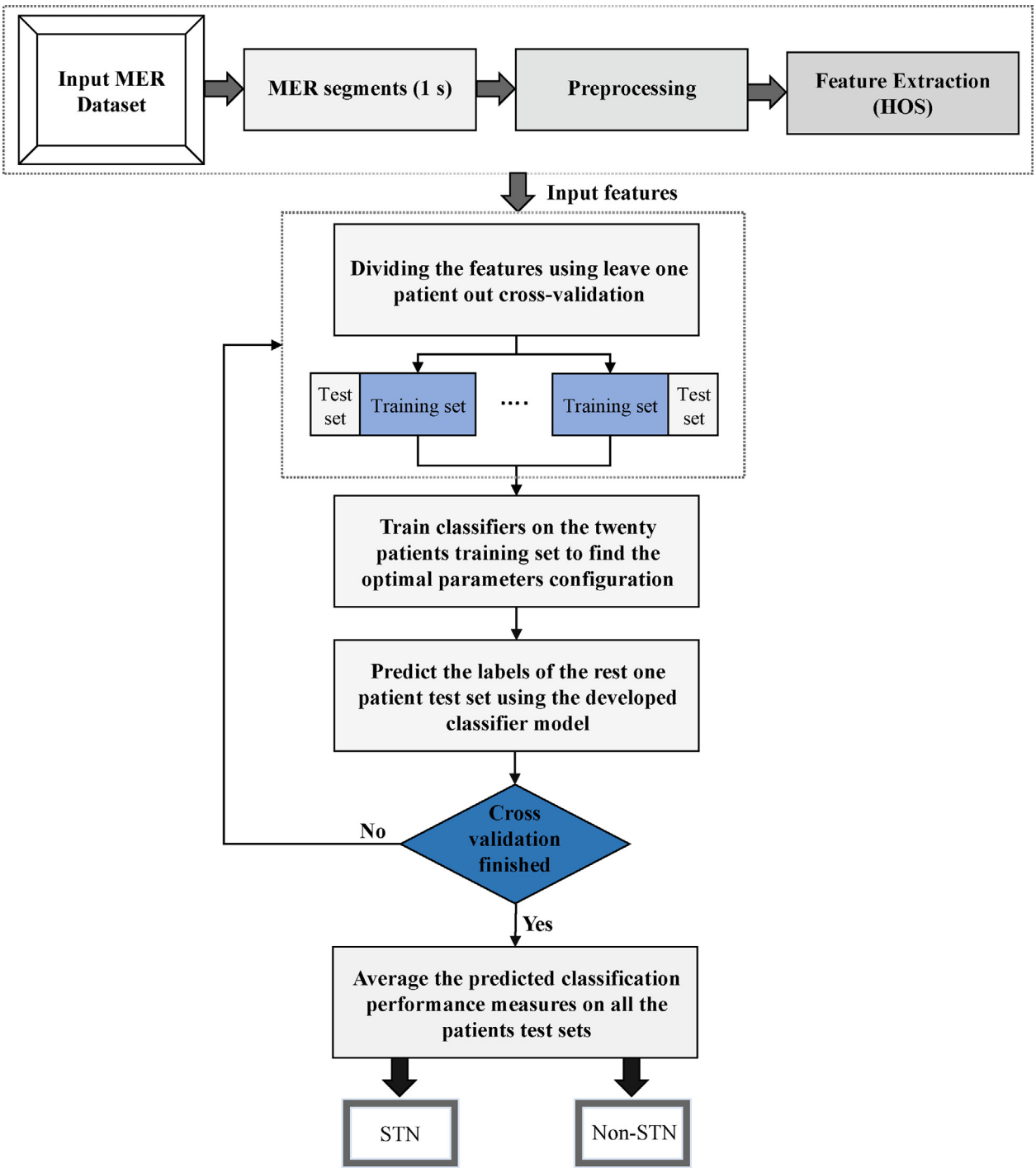

Fig. 1 – Block diagram of the proposed automated STN detection system.

Table 1 – Illustration of the collected MER recordings.

Patients	Pos.	Traj.	STN (s)	non-STN (s)	Total (s)
21	832	39	3206	2067	5273

Pos. = Positions, Traj. = Trajectories.

CT confirming evading of the blood vessels and ventricles. STN coordinates and trajectory are identified through the NeuroNav software using the fused images. Usually the trajectory is designed to penetrate the thalamus (TH), ZI, STN and SNr. MER signals are recorded starting from 10 mm above the predetermined target to below the STN ventral border (i.e. 3–4 mm below the surgical zero-point). Generally, MER electrodes are advanced in 1 mm steps at depth from 10 mm to 5 mm and (0.1–0.5 mm) steps at depth from 5 mm to the end. Neurologist waits for time at each depth before recording to allow artifacts to be resolved. MER signals are assessed intraoperatively by the neurologist to detect the neurophysiological borders of STN. Intraoperative macro-stimulation and postoperative T2 weighted MRI are used to ensure accurate

positioning of DBS electrode inside the optimal target. Subsequently, the internal pulse generator (IPG) is inserted in the chest with established connection to the implanted electrode. All patients had signed the informed consent.

3. Methods

3.1. Preprocessing

The MER signals were separated into 1 s segments. Then, MER segments were high pass filtered using a fifth order Butterworth filter with a cut-off frequency of 0.5 Hz to eliminate any remaining offset and decrease the artifact components. A fifth order zero-phase, non-causal, band-stop Butterworth filter with lower and higher cutoff frequencies of 48 Hz and 52 Hz, in that order, was used to remove the mains 50 Hz noise.

3.2. Feature extraction

3.2.1. Spike dependent and independent

- Standard deviation of the time differences between the spikes of 1s segments.
- Spiking rate: the number of spikes per unit time in each segment.
- Pause index: the ratio of the number of inter-spike intervals higher than 50 ms to the number of those less than 50 ms.
- Pause ratio: the ratio of the cumulative time of inter-spike intervals higher than 50 ms to the total time of those less than 50 ms.
- Teager energy (Ψ): the average of the non-linear energy. Presence of high frequency signals is associated with higher values of this feature, and defined by:

$$\Psi = \frac{1}{N-2}\sum_{i=2}^{N-1} x_i^2 - x_{i-1}x_{i+1} \tag{1}$$

where each x_i is a sample of the data X = ($x_1, x_2, \ldots\ldots, x_n$) and N is the total number of samples in each signal.

- Root mean square (δ): the square root of the mean of the sum of the squares of the signal, and defined by:

$$\delta = \sqrt{\frac{\sum_{i=1}^{N} x_i^2}{N}} \tag{2}$$

- Curve length (L): the sum of succeeding distances between points in 1s MER signal. Unstable values of the signal is associated with higher values of this feature, and defined by:

$$L = \sum_{i=1}^{N-1} |x_{i+1} - x_i| \tag{3}$$

- Zero crossing (ZC): the number of zero crossings in each 1s MER signal, and defined by:

$$ZC = \frac{1}{2}\sum_{i=1}^{N-1} |sgn(x_{i+1}) - sgn(x_i)| \tag{4}$$

- Threshold (γ): the deviation of the data in a window of size N, and defined by:

$$\gamma = \frac{3}{N-1}\sqrt{\sum_{i=1}^{N}(x_i - \overline{X})^2} \tag{5}$$

where $\overline{X}$ is the mean of the data vector.

3.2.2. Wavelet packet decomposition (WPD)

Wavelet analysis has been found very potent in manifesting non-stationary signals [47–49]. WPD, which is a generalization of the traditional WT [50], can optimize the analysis of such signals by producing the frequency content with a flexible resolution [28]. WT decomposes the input signal in the first level by passing it through a series of high and low pass filter banks to yield detail and approximate coefficients, respectively. However, in the subsequent levels, WT decomposes only approximation coefficients of the input signal and detail coefficients are never reanalyzed. As a result, pivotal higher frequency information will be lost. Accordingly, WPD decomposes the detail coefficients of the input signal as well as the approximation coefficients with regard to construct a binary tree of sub-bands. Therefore, 2^n different sets of coefficients emanate from WPD, if level equals n. Consequently, superior frequency resolution is secured by WPD.

In this study, MER signals were decomposed into four levels using WPD with Daubechies 4 mother wavelet. Four statistical parameters: mean, variance, skewness and kurtosis were computed from each sub-band (i.e. 16 sub-bands). Subsequently, 64 WPD based features were calculated. Mean (μ), variance (σ^2), skewness (β_1) and kurtosis (β_2) can be defined by the following mathematical expressions:

$$\mu = \frac{1}{N}\sum_{i=1}^{N} x_i \tag{6}$$

$$\sigma^2 = \frac{1}{N}\sum_{i=1}^{N}(x_i - \mu)^2 \tag{7}$$

$$\beta_1 = \frac{1}{N}\sum_{i=1}^{N}\left(\frac{x_i - \mu}{\sigma}\right)^3 \tag{8}$$

$$\beta_2 = \frac{1}{N}\sum_{i=1}^{N}\left(\frac{x_i - \mu}{\sigma}\right)^4 \tag{9}$$

3.2.3. Higher-order statistics and spectra (HOS)

HOS is a spectral illustration of third and higher order statistics. It is used as a robust tool for preserving the non-linear information of the time series signals [45]. MER signals are expected to have non-linearities in the produced mechanism. Therefore, HOS might provide the advantage of revealing further non-linear and non-Gaussian characteristics of the PD patients MER signals. In this study, a total of 8 bispectrum and 241 cumulants features were extracted from 5273 MER signals.

(i) Bispectrum features: Herein, the bispectrum (third-order spectra) of the signal was calculated owing to its simplicity

(i.e. Higher computational complexity emerges from increasing the order) [43]. Bispectrum which shows symmetry and reflects both the phase coupling degree and the amplitude, can be governed by the following equation:

$$B(f_1,f_2) = E[X(f_1)X(f_2)X^*(f_1+f_2)] \quad (10)$$

where $B(f_1,f_2)$, f_1,f_2 and $X(f)$ denote the bispectrum, the frequency components and the discrete time Fourier transform calculated by FFT [45]. Unlike, conventional power spectrum, bispectrum utilizes FFT with functions of higher order correlation to investigate the presence of quadratic and cubic nonlinear characteristics [44]. Eight features were extracted from the bispectrum namely, the bispectrum mean magnitude (BiMag), the normalized bispectrum standard deviation (BiStd), the normalized bispectral entropy (BiNEnt1), the normalized squared bispectral entropy (BiNEnt2), the bispectrum logarithmic amplitudes summation (L1), the sum of logarithmic amplitudes of the diagonal elements in the bispectrum (L2), the first-order spectral moment of amplitudes of the diagonal elements of the bispectrum (L3) and the second-order spectral moment of amplitudes of the diagonal elements of the bispectrum (L4) [43]. Bispectrum features are beneficial to analyze the MER signals which are non-Gaussian in nature. Epochs of 24000 samples (one second), Hanning window, 50% overlapping, sampling rate of 24 kHz and 512 NFFT points were used to calculate the bispectrum.

(ii) Cumulants features: HOS cumulants are used to discover the higher order relationships that first and second order statistics are not able to establish. Cumulants features are robust to noise, in addition, can capture small changes in the MER signals with the intention of distinguishing STN and non-STN regions. Let x(k) be a digital signal, the n^{th} order cumulants of x(k) can be calculated using the n^{th} order moments. These moments are computed by taking an expectation over the signal multiplied by lagged versions of itself as given below:

$$m_1^x = E[x(k)] \quad (11)$$

$$m_2^x = E[x(k)x(k+T)] \quad (12)$$

$$m_3^x = E[x(k)x(k+T_1)x(k+T_2)] \quad (13)$$

Consequently, the First-, second- and third-order cumulants are governed as follows:

$$C_1^x = m_1^x \quad (14)$$

$$C_2^x(T_1) = m_2^x(T_1) - \left(m_1^x\right)^2 \quad (15)$$

$$C_3^x(T_1,T_2) = m_3^x(T_1,T_2) - m_1^x\left[m_2^x(T_1)+m_2^x(T_2)+m_2^x(T_2-T_1)\right] + 2\left(m_1^x\right)^3 \quad (16)$$

In this work, the third-order cumulants were calculated from each MER signal.

3.3. *Classification*

Various classifiers were tested to estimate the performance of the proposed automated STN localization system. KNN, DT, Boosting and SVM classifiers were used in this study. Extensive search was done to find the optimal parameters configuration for each classifier. The following paragraphs provide a brief illustration of the above mentioned classifiers.

KNN classifier is used to separate data based on the minimum distance, such as, a test sample belongs to a certain class if a more number of this class samples are closer to it compared to other classes samples. KNN relies on the value of K parameter which determines the number of samples used for voting. The lower the K value, the greater the performance in the training set, therefore, K = 1 is the most overfitting case in which every sample is assigned to the nearest neighbor. Despite that higher K values could build more precise and complicated models, generality is not guaranteed.

DT classifier uses the input features to construct a tree-structured model with branches and nodes so as to learn decision rules based on the training data. The test sample class is decided based on these rules. The tree consists of three nodes, internal, root and leaf which reflect the extracted features, the branches decision outcome and the class label (STN or non-STN), respectively [51].

Boosting is an advanced combined classifier based on an ensemble method which attempts to build a strong classifier from a large set of weak classifiers. First create an optimized model based on the training data, then fabricate a new model which try to correct the errors induced by the previous model via emphasizing the misclassified training samples. Models are added until perfect training data error is obtained or assigned maximum number of models is reached. Various algorithms were utilized in this work including AdaBoostM1, Bagging, GentleBoost, LogitBoost and RobustBoost. DT was used as the weak learner in all algorithms [49].

SVM classifier is a simple yet powerful supervised learning approach, insensitive to overtraining and has a good generalization property. It constructs linear or hyperplane separators that maximize the margins (distinction) between the classes. However, when the classes are not linearly separable, kernel functions are employed to address the non-linear classification difficulties in a feature space with higher dimensions [5]. Linear, polynomial (Poly) and radial basis function (RBF) kernels were utilized in this work.

3.4. *Performance measures*

Leave-one-patient-out cross-validation (Leave CV) was used to gauge the performance of the proposed methods. Herein, STN and non-STN MER segments are symbolized as positive and negative class, in that order. True positive (TP) quantifies the number of correctly identified STN segments and false negative (FN) quantifies the number of incorrectly identified STN segments as non-STN. True negative (TN) quantifies the number of correctly identified non-STN segments and false positive (FP) quantifies the number of incorrectly identified non-STN segments as STN. Our MER data contain 5273 signals (1s) where nearly 60% of them are STN (see Table 1). Due to class imbalance in the collected MER data, classification error only is considered as inappropriate performance evaluation criteria. Accordingly, evaluation matrices include accuracy (Acc), sensitivity (Sens), specificity (Spec), Youden's J-statistic (J) and area under the curve (AUC) are employed. Acc, Sens, Spec and J are governed by:

$$Acc = \frac{TP + TN}{TP + TN + FP + FN} \quad (17)$$

$$Sens = \frac{TP}{TP + FN} \quad (18)$$

$$Spec = \frac{TN}{TN + FP} \quad (19)$$

$$J = Sens + Spec - 1 \quad (20)$$

To compute AUC, receiver operating characteristic (ROC) curve is attained by plotting Sens known as true positive rate (TPR) against false positive rate (FPR) of classification for a certain database at various threshold settings. FPR is known as the fall out or probability of false alarm and can be calculated by:

$$FPR = 1 - Spec \quad (21)$$

4. Results

The typical bispectrum magnitude plots of STN and non-STN MER signals are displayed in Figs. 2 and 3. It is evident that the bifrequency magnitude is distinctive for each class, besides, most of the magnitude of the bispectrum is within −0.1 to 0.1. Also, the bispectrum plot declares that there is a random distribution of the magnitudes at several frequencies. Moreover, the bifrequency spread in STN region for PD patients is more complex compared to non-STN region. This may be due to the fact that MER signals originate from STN are more irregular and chaotic. The cumulant contour plots of STN and non-STN MER signals are shown in Figs. 4 and 5. A total of 8 bispectrum and 241 cumulants features were extracted from MER segments of one second. In addition, two existing feature sets containing, 9 spike dependent/independent and 64 WPD based features were extracted (see Section 3.2).

The mean classification performance measures of various classifiers using the existing as well as the proposed features are shown in Table 2. Fig. 6 shows J performance for classifying MER signals using the three feature extraction techniques and all the classifiers. The experimental results showed that HOS gave higher results compared to other feature extraction methods. Also, WPD performed better than SD and SI. Using conventional SD and SI features, LogitBoost achieved the highest mean Acc of 88.81%, Sens of 90.83%, Spec of 86.67%, AUC of 0.8875 and J of 0.7749, followed by AdaBoostM1 which reached Acc of 88.78%, Sens of 90.85%, Spec of 86.51%, AUC of

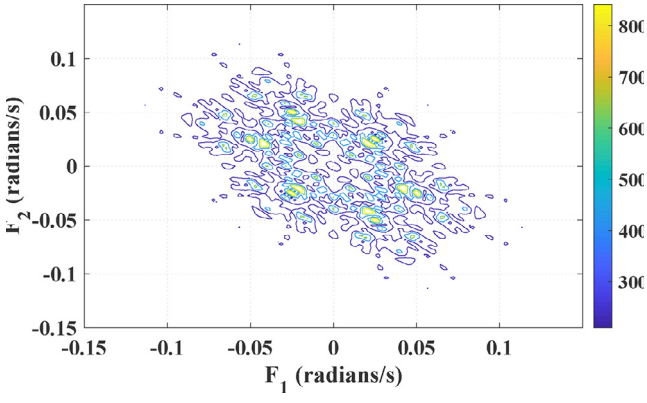

Fig. 2 – HOS Bispectrum plot of the mean of 1000 randomly selected MER signals from STN region.

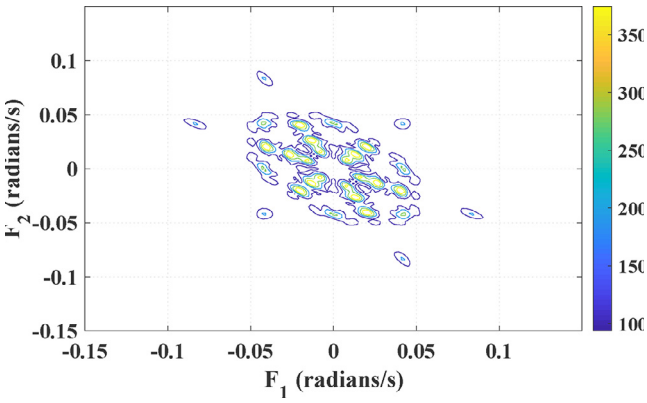

Fig. 3 – HOS Bispectrum plot of the mean of 1000 randomly selected MER signals from non-STN region.

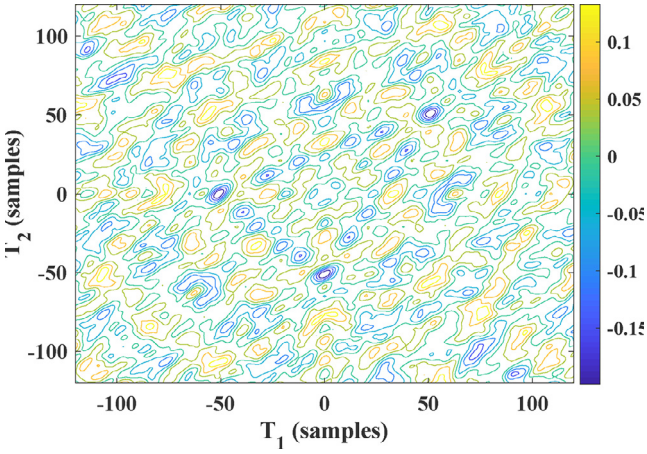

Fig. 4 – HOS Cumulant plot of the mean of 1000 randomly selected MER signals from STN region.

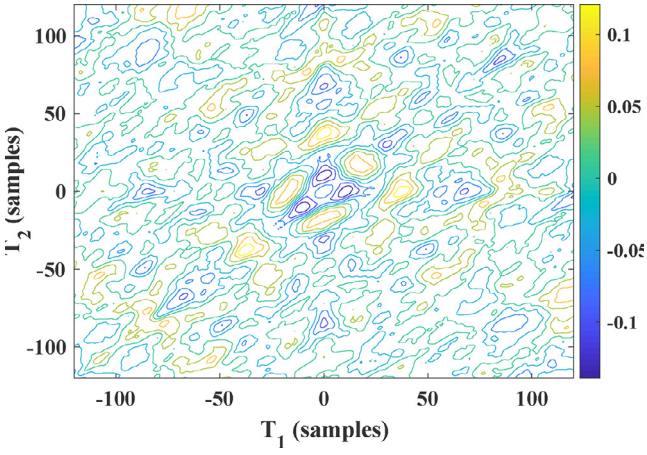

Fig. 5 – HOS Cumulant plot of the mean of 1000 randomly selected MER signals from non-STN region.

0.8868 and J of 0.7737. Similarly, using WPD features as input feature vectors, GentleBoost achieved the highest mean Acc of 93.54%, Sens of 95.03%, Spec of 92.57%, AUC of 0.9380 and J of 0.8760, followed by AdaBoostM1 which reached mean Acc of 93.18%, Sens of 94.39%, Spec of 92.68%, AUC of 0.9354 and J of 0.8707. However, when using HOS features as input feature vectors, SVM with second order Poly kernel (SVM Poly2) achieved the highest mean Acc of 94.81%, Sens of 96.73%, Spec of 92.15%, AUC of 0.9444 and J of 0.8888, followed by LogitBoost which reached mean Acc of 94.45%, Sens of 96.07%, Spec of 92.76%, AUC of 0.9441 and J of 0.8883. It is apparent that SVM Poly2 achieved mean J of 0.7655 and 0.8888 with SD&SI and HOS features, respectively, due to the fact that MER signals are non-linear in nature. Nevertheless, using WPD features, it is noticed that among the different kernels, linear kernel attained the highest performance, such as SVM Linear achieved mean J of 0.8382, which is consistent with the results reported by Karthick et al. [28]. Boosting yielded higher performance than the basic DT using the three feature extraction techniques.

Performance measures including Sens and Spec, which signify that the model can actually distinguish STN versus non-STN classes, are especially relevant. Accordingly, Fig. 7 displays the plot of different measures of the implemented classifiers using HOS features based on Leave CV. Bagging classifier attained the highest performance in separating MER signals stem from STN region, with Sens of 96.81%. On

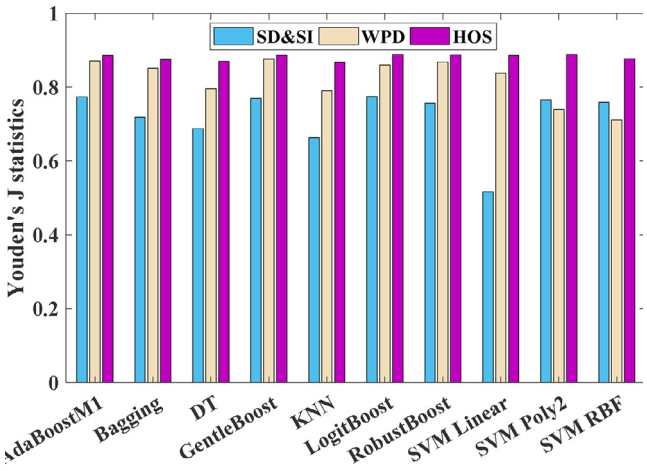

Fig. 6 – The bar plot of performance comparison of each classifier using the three feature extraction techniques in terms of Youden's J-statistic.

Table 2 – The mean of classification measures of higher-order statistics and spectra features in comparison to spike dependent/independent and wavelet packet decomposition features. The validation is implemented using leave-one-patient-out strategy. The mean characterizes average value of 21 patients.

Features	Classifier	Sens (%)	Spec (%)	Acc (%)	AUC	J
SD&SI	KNN	86.14	80.22	83.39	0.8318	0.6635
	DT	88.93	79.87	85.08	0.8440	0.6880
	AdaBoostM1	90.85	86.51	88.78	0.8868	0.7737
	Bagging	90.65	81.30	86.49	0.8598	0.7195
	GentleBoost	90.59	86.38	88.59	0.8848	0.7697
	LogitBoost	90.83	86.67	88.81	0.8875	0.7749
	RobustBoost	90.64	85.07	87.96	0.8786	0.7572
	SVM Linear	85.31	66.34	76.62	0.7582	0.5165
	SVM Poly2	89.76	86.79	88.20	0.8828	0.7655
	SVM RBF	88.79	87.10	87.82	0.8794	0.7589
WPD	KNN	88.68	90.38	89.13	0.8953	0.7905
	DT	90.22	89.44	89.10	0.8983	0.7966
	AdaBoostM1	94.39	92.68	93.18	0.9354	0.8707
	Bagging	95.56	89.62	92.69	0.9259	0.8518
	GentleBoost	95.03	92.57	93.54	0.9380	0.8760
	LogitBoost	91.42	94.65	92.07	0.9303	0.8607
	RobustBoost	93.73	93.10	92.91	0.9341	0.8683
	SVM Linear	94.51	89.31	92.39	0.9191	0.8382
	SVM Poly2	88.22	85.73	87.19	0.8698	0.7395
	SVM RBF	89.56	81.59	86.56	0.8558	0.7115
HOS	KNN	94.29	92.41	93.28	0.9335	0.8670
	DT	95.70	91.33	93.71	0.9352	0.8703
	AdaBoostM1	95.95	92.64	94.36	0.9430	0.8860
	Bagging	96.81	90.71	94.23	0.9376	0.8752
	GentleBoost	95.70	93.02	94.32	0.9436	0.8872
	LogitBoost	96.07	92.76	94.45	0.9441	0.8883
	RobustBoost	95.63	93.14	94.37	0.9438	0.8877
	SVM Linear	96.23	92.39	94.42	0.9431	0.8862
	SVM Poly2	96.73	92.15	94.81	0.9444	0.8888
	SVM RBF	94.60	93.10	93.78	0.9385	0.8770

the other hand, RobustBoost classifier yielded the highest performance in separating MER signals stem from non-STN region, with Spec of 93.14%. It is clear that, HOS bispectrum and cumulants are effective for all the classifiers. HOS features extraction and classification of one second MER signal take mean processing time of 1.14 and 0.0083 s, in that order. This work was executed using a PC with Intel Core i7 (2.20 GHz) processor and 8-GB RAM. The entire system was conducted using MATLAB R2019a environment.

5. Discussion

In spite of advancement in imaging modalities [22], the vast majority of DBS centers still use MER to validate the planned trajectories [23,24,18]. Meanwhile, MER signals analysis has been increasingly proved to provide vital neuronal biomarkers to discriminate between the different structures in the BG region [19,28]. Though, until now, it is still uncertain which features can be more crucial to expose significant information regarding STN region. Overall, several linear and frequency-domain techniques have been exploited to analyze MER signals and define new signatures of STN region in PD patients, however such techniques are not effective to recognize the delicate changes in MER signals owing to their chaotic, non-linear and complex nature [19]. Besides, STN region is associated with more irregular MER signals [41]. Despite that, the hidden key signatures of stochastic non-stationary signals could be unearthed by using non-linear algorithms, since they have the ability to capture momentary changes associated with different properties, for instance, reliability, similarity, sensitivity and predictability of the signal [43,45]. This would help to explore the non-linear components existing in the MER signals. Therefore, in this study, the presented approach is tailored towards the automated detection of STN borders using non-linear HOS based features extracted from MER signals. To accentuate, the novelty of this work is the formulation of unique HOS plots for STN and non-STN regions.

Table 3 lists summary of the previous works carried out in order to detect STN region in PD patients based on MER signals. A similar stable dataset is usually a critical demand for subsequent successful analysis of features and classification [25]. Though, MER signals homogeneity is affected by different recording machine parameters, variable electrodes impedance and discrepancy of inter-patient neurophysiology, which would induce possible unstable features (i.e. High variation in amplitude of all cases) and large classification errors [31,42]. Accordingly, authors in [25,33,36,38] employed a specially-designed feature standardization and normalization to remove outliers and assign the feature vectors to a certain range of values. Nevertheless, the caveat is that calculation of features in this regard requires the MER data to be collected first prior to implementation. As a result, normalization based approaches are feasible for postoperative assessment, but they are not practical for real time applications and cannot aid the neurosurgeon intraoperatively [39]. Furthermore, normalization of MER signals may lead to loss of pivotal information, for instance, high-frequency portions and background neural activity properties which would introduce some uncertainty to the system accuracy [42].

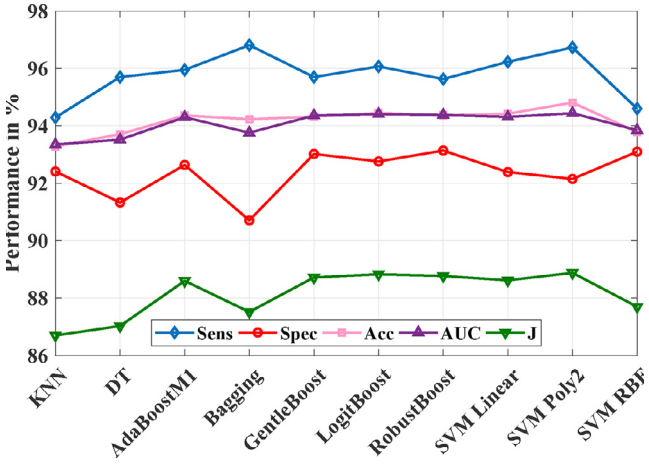

Fig. 7 – The average of performance measures of each classifier using HOS features across 21 patients cross-validation set.

It is important to mention that 10-fold cross-validation (10-fold CV) was used to estimate the classification performance in the previous works [31,35,36,39,46]. In this technique, the data are regularly divided into 10 subsets of equal size. After that, classifier is trained and tested for 10 rounds (folds), where in each round one subset is used for testing while the other nine subsets are used for training, then the average testing error over the 10 rounds is the final classification error. However, 10-fold CV is not enough to gauge the performance as training and testing data through various folds may include signals from the same trajectory or from the same position in case of segmentation. This will very likely increase the bias in favor of training and testing sets and thereby artificially improve the classification performance [25,38]. To mitigate such encumbrance, Leave CV was used to gauge the performance of the adopted classifiers.

It can be observed that several studies have applied different normalization and/or feature selection techniques [25,33,36,38,37,52]. However, this work flow suffers from several disadvantages as it cannot be implemented intraoperatively and may open the door for design errors. In addition, these models often suffer from biasing and furnish lower performance when validated on bigger datasets. Meantime, researchers exploited HOS methods in various applications [43–45]. Nevertheless, automatic STN detection in MER signals using HOS received less attention. Herein, a non-linear architecture to classify the MER signals into STN and non-STN classes is developed. To the best of authors knowledge, this is the first attempt at detecting the dorsal and ventral borders of STN using HOS. Additionally, unlike the previous studies, no normalization or feature selection techniques are necessitated, such as all the extracted features demonstrate crucial characteristics of the STN region. Consequently, the proposed HOS model is minimalist: that the automated decision support is only based on the extracted features without any information reduction by feature selection.

Also, it can be noticed that most of the studies [25,30,31,33,35–38] used SD features to localize the STN region. However, these features are subject to computational complications and errors, particularly when calculated in real

Table 3 – Summary of studies conducted on automated detection of STN.

Authors	Patients No.	Feature extraction	Classifier	Performance(%)
Wong et al. [33]	27	7 SD + 6 SI; Feature Norm.	Fuzzy clustering + Activity map	Sens = 90 (STN entry); Sens = 95 (STN exit)
Cagnan et al. [30]	48	Firing rate + Background neural activity + PSD	Unsupervised algorithm	Acc = 88 (42–258 Traj. Training–Testing)
Chaovalitwongse et al. [25]	17	7 SD + 6 SI; Feature Norm.	Bayesian + DT + KNN	Acc = 89.6 (Leave CV)
Guillen et al. [46]	4	6 SI	SVM	Acc = 99.4 (10-fold CV)
Vargas Cardona et al. [42]	4	Inter spike interval + Adaptive wavelets + Wavelet Transform	Bayesian + KNN	Sens = 85
Ciecierski et al. [31]	NR	SD attributes + Background neural features	RSES + RF	Acc = 97.6 (10-fold CV)
Rajpurohit et al. [36]	26	7 SD + 6 SI; Feature selection: Forward, Backward; Patient-specific Norm.	LR + KNN + SVM + Gaussian Nave Bayes	Acc = 84 (10-fold CV)
Schiaffio et al. [35]	8	Data Norm.; 8 SD + 7 SI	KNN + Fuzzy KNN	Sens = 72 Spec = 82 (Leave CV)
Schiaffio et al. [37]	15	8 SD + 8 SI; Feature selection: Branch and Bound, ReliffF, LASSO, ELASTIC Net	KNN	Acc = 86.13 (10-fold CV)
Valsky et al. [29]	81	Normalized root mean square + PSD	SVM + HMM	Acc = 94 (58–73 Traj. Training–Testing)
Vargas Cardona et al. [27]	Set(A):6; Set(B):4	Adaptive wavelets + WT + ISI	Multi-task Gaussian process regression with CMOC, LMC and IMC covarainces + KNN + SVM + LDC + QDC + Gaussian	Dataset(A): Acc = 85.99 (Leave CV) Dataset (B): Acc = 84.1 (Leave CV)
Bellino et al. [38]	14	10 SD + 8 SI; Patient-specific Norm. + Hemisphere-specific Norm.; Feature selection: ReliefF, Backward, Forward,,Branch and Bound	Naive Bayes + KNN + DT	Acc = 94.35 (Leave CV)
Karthick et al. [41]	26	Discrete wavelet decomposition	RF	Acc = 83 (Leave CV)
Khosravi et al. [40]	50	FFT	K-means clustering + SOM	Acc = 80
Karthick et al. [28]	26	WPD	RF + SVM + KNN	Acc = 94 (Leave CV)
This work	**21**	**SD&SI + WPD + HOS**	**KNN + DT + Boosting + SVM**	**Acc = 94.81 (Leave CV)**

No. = Number, Traj. = Trajectories, Norm. = Normalization, SD = Spike Dependent, SI = Spike Independent, NR = Not Reported.

time [29]. In addition, precise spike detection hinges on longer recording duration, high signal to noise ratio as well as stationary electrodes. As a result, the complexity and time of the surgery would increase [19]. Also, Cao et al. [52] reported that the features extracted from the background unit activity are representative and able to detect the dorsal and ventral borders of the STN. Moreover, Ciecierski et al. [31] concluded that utilizing a combination of SD and SI features yields a significant improvement rather than using SD features alone, because each single feature group can just reflect one-side characteristics of the electrophysiological activity. Though, employing all the SD and SI features could cause information imbalance, as the contribution of each feature is uncertain [52]. Consequently, following feature selection [36,40], the nine SD and SI features, reported in [36,40,46] as informative and able to expose the biomarkers of STN region, were extracted in this study. Also, authors in [28] reported that WPD exhibits additional information of low and high frequency components attributable to the fact that WT tree is subset of WPD tree, as discussed earlier. They demonstrated that fixed frequency bandwidth features would ameliorate the performance and maintain more accurate representation and higher resolution. Therefore, WPD features based on the study by Karthick et al. [28] were extracted here. The two aforementioned feature groups were employed to validate the performance of the designed bispectrum and cumulants features.

The HOS of MER signals reveals essential information of higher order relationships and deviation from Gaussianity. Two HOS methods (bispectrum and cumulants) have shown great stability in the analysis of non-stationary signals [45]. Moreover, HOS features are robust enough to investigate noisy signals, thus, the HOS methods are suitable for MER signal study. The proposed HOS features are found to be the most representative feature group to identify the neurophysiological borders of STN. Such as, SD and SI features accomplished mean AUC between 0.7582 and 0.8875, while WPD features yielded mean AUC between 0.8558 and 0.9380. Mean AUC between 0.9335 and 0.9444 were achieved by HOS features (see Table 2). Despite having limited number of PD patients in our dataset, SVM Poly2 achieved promising performance with Acc of 94.81%, AUC of 0.9444 and J of 0.8888 using bispectrum and cumulants features which is encouraging for automated STN detection.

The motivation behind using short segments (1s) of MER signals was to reduce the listening time, so as the neurologist is not required to spend a long time listening to the MER at each position for the detection of STN region. Also, the choice of such short signals is enough to extract meaningfully discriminating features and provide a good balance between concision and capacity to achieve precise predictions [35,27,46]. MATLAB software was used to implement the proposed method, which can be installed in hospitals to help the process of STN localization. The limitation of this work is that the proposed method needs to be evaluated with a larger dataset, such as MER signals from only 21 PD patients were used in this study. In order to fabricate a reliable automated system for the identification of STN borders, huge database from several DBS centers is required.

6. Conclusion

Recently, revealing of STN signatures has received the attention of many researchers. Therefore, this study proposed a supervised classification model for detection of the neurophysiological borders of STN based on HOS features extracted from MER signals. The presented results demonstrate that SVM Poly2 classifier is able to characterize STN and non-STN regions in 21 PD patients with an average Acc, Sens, Spec, AUC and J of 94.81%, 96.73%, 92.15%, 0.9444 and 0.8888. In addition, we experimentally showed that HOS achieved higher performance than the commonly used methods (i.e SD, SI and WPD) due to the ability to expose the underlying hidden non-linear features and extract details regarding phase relations from MER signals without any information reduction. Consequently, the proposed method is robust and can accurately identify one second MER recordings stem from STN region. Hence, the developed MER based automated system could greatly be regarded from a clinical perspective as an efficient tool for STN detection in PD patients.

For future work, the proposed methodology can be further extended for localization of other subcortical targets in the BG area, for instance, GPi. Finally, the enhancement of the proposed method requires further investigation on higher number of patients.

CRediT authorship contribution statement

Mohamed Hosny: Methodology, Software, Visualization, Validation, Writing - original draft, Writing - review & editing. **Minwei Zhu:** Resources, Data curation. **Wenpeng Gao:** Conceptualization, Project administration, Funding acquisition, Writing - review & editing. **Yili Fu:** Supervision.

Declaration of Competing Interest

The authors declare that they have no known competing financial interests or personal relationships that could have appeared to influence the work reported in this paper.

Acknowledgments

This work was supported by the National Natural Science Foundation of China (Grant No. 81201150). It was also supported by Postdoctoral Scientific Research Developmental Fund of Heilongjiang Province of China (Grant No. LBH-Q17012) and Natural Science Foundation of Heilongjiang Province of China (Grant No. LH2019F021).

REFERENCES

[1] Soares MI, Soares-Dos-Reis R, Rosas MJ, Monteiro P, Massano J. Intraoperative microelectrode recording in Parkinson's disease subthalamic deep brain stimulation: Analysis of clinical utility. J Clin Neurosci 2019;69:104–8.

[2] Zhang Y, Xu S, Xiao G, Song Y, Gao F, Wang M, et al. High frequency stimulation of subthalamic nucleus

synchronously modulates primary motor cortex and caudate putamen based on dopamine concentration and electrophysiology activities using microelectrode arrays in Parkinson's disease rats. Sens Actuat B Chem 2019;301(June) 127126.
[3] Zhang S, Song Y, Wang M, Xiao G, Gao F, Li Z, et al. Real-time simultaneous recording of electrophysiological activities and dopamine overflow in the deep brain nuclei of a non-human primate with Parkinson's disease using nano-based microelectrode arrays. Microsyst Nanoeng 2018;4(1):17070.
[4] Bonnevie T, Zaghloul KA. The subthalamic nucleus: unravelling new roles and mechanisms in the control of action. The Neuroscientist 2019;25(1):48–64.
[5] Nilashi M, Ibrahim O, Ahmadi H, Shahmoradi L, Farahmand M. A hybrid intelligent system for the prediction of Parkinson's Disease progression using machine learning techniques. Biocybern Biomed Eng 2018;38(1):1–15.
[6] Velisar A, Syrkin-Nikolau J, Blumenfeld Z, Trager M, Afzal M, Prabhakar V, et al. Dual threshold neural closed loop deep brain stimulation in Parkinson disease patients. Brain Stimulat 2019;12(4):868–76.
[7] Alper MA, Goudreau J, Daniel M. Pose and Optical Flow Fusion (POFF) for accurate tremor detection and quantification. Biocybern Biomed Eng 2020;40(1):468–81.
[8] Copur EH, Freeman CT, Chu B, Laila DS. Repetitive control of electrical stimulation for tremor suppression. IEEE Trans Control Syst Technol 2019;27(2):540–52.
[9] Kwon Y, Park SH, Kim JW, Ho Y, Jeon HM, Bang MJ, et al. Quantitative evaluation of parkinsonian rigidity during intra-operative deep brain stimulation. Bio-Med Mater Eng 2014;24 (6):2273–81.
[10] Chen KHS, Chen R. Invasive and noninvasive brain stimulation in Parkinson's disease: clinical effects and future perspectives. Clin Pharmacol Therapeut 2019;106(4):763–75.
[11] Boller JK, Barbe MT, Pauls KAM, Reck C, Brand M, Maier F, et al. Decision-making under risk is improved by both dopaminergic medication and subthalamic stimulation in Parkinson's disease. Exp Neurol 2014;254:70–7.
[12] Barbe MT, Tonder L, Krack P, Debû B, Schüpbach M, Paschen S, et al. Deep brain stimulation for freezing of gait in Parkinson's disease with early motor complications. Movement Disorders 2020;35(1):82–90.
[13] Heo JH, Jeon HM, Choi EB, Kwon DY, Eom GM. Effect of sensory electrical stimulation on resting tremors in patients with Parkinson's disease and Swedds. J Mech Med Biol 2019;19(7):1940033 (9 p). .
[14] Khawaldeh S, Tinkhauser G, Shah SA, Peterman K, Debove I, Nguyen TAK, et al. Subthalamic nucleus activity dynamics and limb movement prediction in Parkinson's disease. Brain: A J Neurol 2020;143(2):582–96.
[15] Mao Z, Ling Z, Pan L, Xu X, Cui Z, Liang S, et al. Comparison of efficacy of deep brain stimulation of different targets in Parkinson's disease: a network meta-analysis. Front Aging Neurosci 2019;11(FEB):1–8..
[16] Valsky D, Blackwell KT, Tamir I, Eitan R, Bergman H, Israel Z. Real-time machine learning classification of pallidal borders during deep brain stimulation surgery. J Neural Eng 2020;17 (1).
[17] Dideriksen JL, Laine CM, Dosen S, Muceli S, Rocon E, Pons JL, et al. Electrical stimulation of afferent pathways for the suppression of pathological tremor. Front Neurosci 2017;11 (APR):1–11..
[18] Mehanna R, Machado AG, Connett JE, Alsaloum F, Cooper SE. Intraoperative microstimulation predicts outcome of postoperative macrostimulation in subthalamic nucleus deep brain stimulation for Parkinson's disease. Neuromodulation 2017;20(5):456–63.
[19] Rui K, Maszczyk T, An A, See Q, Dauwels J, Kon N, et al. A review on microelectrode recording selection of features for machine learning in deep brain stimulation surgery for Parkinson ' s disease. Clin Neurophysiol 2019;130 (1):145–54.
[20] Farrokhi F, Buchlak QD, Sikora M, Esmaili N, Marsans M, McLeod P, et al. Investigating risk factors and predicting complications in deep brain stimulation surgery with machine learning algorithms. World Neurosurg 2020;134:468–81.
[21] Horn A, Neumann WJ, Degen K, Schneider GH, Kühn AA. Toward an electrophysiological "sweet spot" for deep brain stimulation in the subthalamic nucleus. Human Brain Map 2017;38(7):3377–90.
[22] Shamir RR, Duchin Y, Kim J, Patriat R, Marmor O, Bergman H, et al. Microelectrode recordings validate the clinical visualization of subthalamic-nucleus based on 7T magnetic resonance imaging and machine learning for deep brain stimulation surgery. Clin Neurosurg 2019;84(3):749–56.
[23] Kocabicak E, Alptekin O, Aygun D, Yildiz O, Temel Y. Microelectrode recording for deep brain stimulation on the subthalamic nucleus in patients with advanced Parkinsons diesease: advantage or loss of time. Turk Neurosurg 2019;29 (5):677–82.
[24] Hartmann CJ, Fliegen S, Groiss SJ, Wojtecki L, Schnitzler A. An update on best practice of deep brain stimulation in Parkinsons disease. Therapeut Adv Neurol Disorders 2019;12:1–20.
[25] Chaovalitwongse W, Jeong Y, Jeong MK, Danish S, Wong S. Pattern recognition approaches for identifying subcortical targets during deep brain stimulation surgery. IEEE Intell Syst 2011;26(5):54–63.
[26] Hosny M, Zhu M, Gao W, Fu Y. A novel deep LSTM network for artifacts detection in microelectrode recordings. Biocybern Biomed Eng 2020;40(3):1052–63.
[27] Vargas Cardona HD, Álvarez MA, Orozco ÁA. Multi-task learning for subthalamic nucleus identification in deep brain stimulation. Int J Mach Learn Cybern 2018;9(7):1181–92.
[28] Karthick PA, Wan KR, An Qi AS, Dauwels J, King NKK. Automated detection of subthalamic nucleus in deep brain stimulation surgery for parkinson's disease using microelectrode recordings and wavelet packet features. J Neurosci Methods 2020;343(June):108826..
[29] Valsky D, Marmor-Levin O, Deffains M, Eitan R, Blackwell KT, Bergman H, et al. Stop! border ahead: Automatic detection of subthalamic exit during deep brain stimulation surgery. Movement Disorders 2017;32(1):70–9.
[30] Cagnan H, Dolan K, He X, Contarino MF, Schuurman R, Van Den Munckhof P, et al. Automatic subthalamic nucleus detection from microelectrode recordings based on noise level and neuronal activity. J Neural Eng 2011;8(4):046006 (9 p). .
[31] Ciecierski K, Mandat T, Rola R, Raś ZW, Przybyszewski AW. Computer aided subthalamic nucleus (stn) localization during deep brain stimulation (dbs) surgery in parkinson's patients. Annales Academiae Medicae Silesiensis 2014;5 (68):275–83.
[32] Farokhniaee AA, McIntyre CC. Theoretical principles of deep brain stimulation induced synaptic suppression. Brain Stimulat 2019;12(6):1402–9.
[33] Wong S, Baltuch GH, Jaggi JL, Danish SF. Functional localization and visualization of the subthalamic nucleus from microelectrode recordings acquired during DBS surgery

with unsupervised machine learning. J Neural Eng 2009;6 (2):026006 (11 p). .
[34] Ciecierski KA, Mandat T. Unsupervised machine learning in classification of neurobiological data. Intelligent methods and big data in industrial applications. Springer International Publishing; 2019..
[35] Schiaffino L, Rosado Munoz A, Guerrero Martinez J, Francés Villora J, Gutiérrez A, Martinez Torres I, et al. STN area detection using K-NN classifiers for MER recordings in Parkinson patients during neurostimulator implant surgery. J Phys Conf Ser 2016;705(1):441–4.
[36] Rajpurohit V, Danish SF, Hargreaves EL, Wong S. Optimizing computational feature sets for subthalamic nucleus localization in DBS surgery with feature selection. Clin Neurophysiol 2015;126(5):975–82.
[37] Schiaffino L, Muñoz AR, Villora JF, Bataller M, Gutiérrez A, Torres IM. Feature selection for knn classifier to improve accurate detection of subthalamic nucleus during deep brain stimulation surgery in parkinson's patients. In: VII Latin American Congress on Biomedical Engineering CLAIB, Bucaramanga, Santander, Colombia; vol. 60 of IFMBE Proceedings. Springer; 2017. pp. 441–4. .
[38] Bellino G, Schiaffino L, Battisti M, Guerrero J, Rosado-Muñoz A. Optimization of the KNN supervised classification algorithm as a support tool for the implantation of deep brain stimulators in patients with Parkinson's disease. Entropy 2019;21(4):346.
[39] Khosravi M, Atashzar SF, Gilmore G, Jog MS, Patel RV. Electrophysiological signal processing for intraoperative localization of subthalamic nucleus during deep brain stimulation surgery. In: IEEE Global Conference on Signal and Information Processing, GlobalSIP. IEEE; 2019. pp. 424–8. .
[40] Khosravi M, Atashzar SF, Gilmore G, Jog MS, Patel RV. Unsupervised clustering of micro-electrophysiological signals for localization of subthalamic nucleus during DBS surgery. In: International IEEE/EMBS Conference on Neural Engineering, NER. IEEE; 2019. pp. 17–20. .
[41] Karthick PA, Wan KR, Yuvaraj R, See AA, King NKK, Dauwels J. Detection of subthalamic nucleus using time-frequency features of microelectrode recordings and random forest classifier. In: 41st Annual International Conference of the IEEE Engineering in Medicine and Biology Society (EMBC). IEEE; 2019. p. 4164–7.
[42] Vargas Cardona HD, Padilla JB, Arango R, Carmona H, Alvarez MA, Guijarro Estelles E, et al. NEUROZONE: On-line recognition of brain structures in stereotactic surgery - application to Parkinson's disease. In: Annual International Conference of the IEEE Engineering in Medicine and Biology Society; vol. 103. IEEE; 2012. pp. 2219–22. .
[43] Yuvaraj R, Rajendra Acharya U, Hagiwara Y. A novel Parkinson's disease diagnosis index using higher-order spectra features in EEG signals. Neural Comput Appl 2018;30 (4):1225–35.
[44] Bou Assi E, Gagliano L, Rihana S, Nguyen DK, Sawan M. Bispectrum features and multilayer perceptron classifier to enhance seizure prediction. Sci Rep 2018;8(1):1–8.
[45] Acharya UR, Sudarshan VK, Koh JE, Martis RJ, Tan JH, Oh SL, et al. Application of higher-order spectra for the characterization of Coronary artery disease using electrocardiogram signals. Biomed Signal Process Control 2017;31:31–43.
[46] Guillén P, Martinez-De-Pisón F, Sánchez R, Argáez M, Velázquez L. Characterization of subcortical structures during deep brain stimulation utilizing support vector machines 2011:7949–52.
[47] Nawaz R, Cheah KH, Nisar H, Yap VV. Comparison of different feature extraction methods for EEG-based emotion recognition. Biocybern Biomed Eng 2020;40(3):910–26.
[48] Sawant NK, Patidar S, Nesaragi N, Acharya UR. Automated detection of abnormal heart sound signals using Fano-factor constrained tunable quality wavelet transform. Biocybern Biomed Eng 2021;41(1):111–26.
[49] Tor HT, Ooi CP, Lim-Ashworth NS, Wei JKE, Jahmunah V, Oh SL, et al. Automated detection of conduct disorder and attention deficit hyperactivity disorder using decomposition and nonlinear techniques with EEG signals. Comput Methods Program Biomed 2021;200 105941.
[50] El Bahy M, Hosny M, Mohamed WA, Ibrahim S. EEG signal classification using neural network and support vector machine in brain computer interface. In: International Conference on Advanced Intelligent Systems and Informatics. Springer; 2016. p. 246–56.
[51] Acharya UR, Hagiwara Y, Koh JEW, Oh SL, Tan JH, Adam M, et al. Entropies for automated detection of coronary artery disease using ECG signals: A review. Biocybern Biomed Eng 2018;38(2):373–84.
[52] Cao L, Jie L, Zhou Y, Liu Y, Liu H. Automatic feature group combination selection method based on GA for the functional regions clustering in DBS. Comput Methods Program Biomed 2020;183.